

Segment then Splat: A Unified Approach for 3D Open-Vocabulary Segmentation based on Gaussian Splatting

Yiren Lu, Yunlai Zhou, Yiran Qiao, Chaoda Song, Tuo Liang, Jing Ma, Yu Yin
Case Western Reserve University

{yiren.lu, yunlai.zhou, yiran.qiao, chaoda.song, tuo.liang, jing.ma5, yu.yin}@case.edu

<https://vulab-ai.github.io/Segment-then-Splat/>

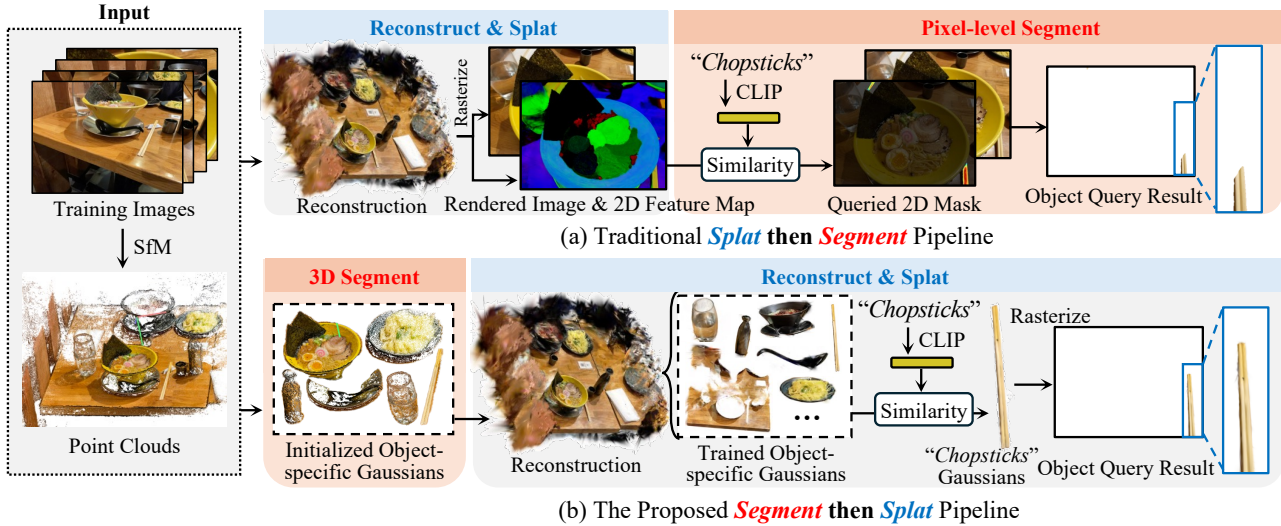


Figure 1. **Comparison of our Segment-then-Splat pipeline and the traditional Splat-then-Segment approach.** (a) The traditional Splat-then-Segment pipeline learns a language field alongside the reconstruction of the entire scene. During object queries, it renders Gaussian language embeddings into a 2D feature map to identify relevant pixels based on the input text embedding. (b) In contrast, our Segment-then-Splat pipeline first initialize Gaussians into object-specific sets before reconstruction, ensuring a more precise object-Gaussian correspondence and improving segmentation accuracy.

Abstract

Open-vocabulary querying in 3D space is crucial for enabling more intelligent perception in applications such as robotics, autonomous systems, and augmented reality. However, most existing methods rely on 2D pixel-level parsing, leading to multi-view inconsistencies and poor 3D object retrieval. Moreover, they are limited to static scenes and struggle with dynamic scenes due to the complexities of motion modeling. In this paper, we propose **Segment then Splat**, a 3D-aware open vocabulary segmentation approach for both static and dynamic scenes based on Gaussian Splatting. **Segment then Splat** reverses the long established approach of “segmentation after reconstruction” by dividing Gaussians into distinct object sets before reconstruction. Once the reconstruction is complete, the scene is naturally segmented into individual objects, achieving

true 3D segmentation. This approach not only eliminates Gaussian-object misalignment issues in dynamic scenes but also accelerates the optimization process, as it eliminates the need for learning a separate language field. After optimization, a CLIP embedding is assigned to each object to enable open-vocabulary querying. Extensive experiments on various datasets demonstrate the effectiveness of our proposed method in both static and dynamic scenarios.

1. Introduction

3D open vocabulary querying marks a pivotal step in language-driven interaction with 3D environments, removing the need for predefined labels. This capability is vital for large-scale scene exploration, understanding and editing [3, 16, 29, 30], robotic navigation [7, 19] and manipulation [23, 27], where free-form text bridges human language and

machine perception.

3D Gaussian Splatting (3DGS) [8] has been a widely adopted 3D representation due to its efficient training and real-time rendering capabilities. While 3DGS has demonstrated remarkable performance in scene reconstruction and novel view synthesis, it lacks inherent semantic understandings, limiting its applicability in tasks that require natural language-driven retrieval and reasoning.

To solve this issue, most existing works [9, 21, 28, 36] incorporate a separate language field alongside Gaussian Splatting reconstruction. By rendering the language field into 2D feature maps, they enable pixel-based querying by retrieving relevant pixels based on the input text embedding. However, this approach essentially performs segmentation in 2D space rather than partitioning Gaussians in 3D space, leading to several drawbacks: 1) **Inconsistent 2D segmentation** results across different views, leading to inaccurate object boundaries. 2) **Failure to learn the actual 3D information** of objects, making object extraction in 3D challenging and limiting downstream tasks like robot navigation and 3D manipulation. 3) **Inapplicability to dynamic scenes**, since Gaussians may have varying semantic meanings at different time steps, preventing straightforward extensions to time-varying or moving objects.

Recently, a few works [6, 32] have explored direct segmentation in 3D space. However, these approaches require a predefined number of objects for clustering [32] or are limited to foreground segmentation [6], and also cannot be directly applied to dynamic scenes.

Despite the differences in segmentation strategies, whether pixel-based or 3D-based, all existing approaches follow a “reconstruction-then-segmentation” (*i.e.* splat then segment) paradigm. This approach inherently results in imprecise object boundaries, as each Gaussian may encode geometric and semantic information from multiple objects, leading to segmentation ambiguity.

In this paper, we propose *Segment then Splat*, a unified framework for 3D-aware open-vocabulary segmentation that can be applied to both static and dynamic scenes. Unlike existing methods that adopt a “splat then segment” approach, our method reverses the process by first initializing each object with a specific set of Gaussians, as shown in Fig. 1. During training, each set of Gaussians is assigned a unique object ID and contributes only to its corresponding object, guided by 2D multi-view mask supervision. By doing so, each Gaussian is dedicated to a single object and thus learns more accurate object geometry. Moreover, since the Gaussian-object correspondence is strictly maintained, our method can be directly applied to dynamic scenes without the risk of Gaussian-object misalignment (*i.e.* one Gaussian may represent different objects at different time steps). Finally, *Segment then Splat* requires only one pass of reconstruction and does not depend on learning an additional fea-

ture field, significantly improving efficiency. In summary, our key contributions include:

- We propose *Segment then Splat*, a unified framework for 3D-aware open-vocabulary segmentation based on Gaussian Splatting.
- We design a “segmentation then reconstruction” pipeline that enhances object geometry, ensures compatibility with dynamic scenes, and eliminates the need to learn a separate feature field.
- We introduce a robust object-tracking module capable of mitigating tracking errors in complex scenes.
- Extensive experiments on diverse static and dynamic datasets demonstrate the superior performance of our method in 3D object segmentation.

2. Related Work

2.1. 3D & 4D Gaussian Splatting

3D Gaussian Splatting (3DGS) [8] is a widely recognized 3D scene representation that introduces anisotropic 3D Gaussians and an efficient differentiable splatting scheme. This enables high-quality explicit scene representation with efficient training and real-time rendering. However, since it was originally designed for static scenes, 3DGS lacks the capability to model dynamic environments.

To address this limitation, many researches focus on how to better model scene dynamics [2, 14, 17, 18, 31, 33, 34]. 4D Gaussian Splatting [34] directly extends 3DGS into four dimensions to facilitate dynamic scene reconstruction. Meanwhile, Deformable-3D-Gaussians [33] leverages a multi-layer perceptron (MLP) to learn per-timestamp positions, rotations, and scales for each Gaussian, effectively capturing object motion and deformation over time. 4DGaussians [31] utilizes multi-resolution HexPlanes [2] to decode features for temporal deformation of 3D Gaussians, while STG [14] encodes changes over time via a temporal opacity term and a polynomial function for each Gaussian, yielding a more detailed representation of dynamic scenes.

Despite these advancements, the above methods act solely as scene representations. After reconstruction, they do not support additional interaction or provide information beyond geometry and texture. In contrast, our approach integrates CLIP [22] embeddings into Gaussian Splatting, assigning each Gaussian an object-level semantic meaning. This capability enables open-vocabulary segmentation, allowing users to retrieve, organize, and query objects within the reconstructed scene through natural language prompts.

2.2. Language Embedded Scene Representation

Various research has focused on integrating language features [9, 28, 35, 37] into 3D scene representations. LERF [9] pioneered this approach by embedding CLIP features in NeRF. Specifically, it extracts pixel-level CLIP embed-

dings from multi-scale image crops and trains them alongside NeRF to enable open-vocabulary 3D queries. Building on this idea, LEGaussians [28] incorporates uncertainty and semantic feature attributes into each Gaussian, while introducing a quantization strategy to compress high-level language and semantic features. LangSplat [21] employs a scene-wise language autoencoder to learn language features within a scene-specific latent space, and incorporate SAM mask to enable clear object boundaries in rendered feature images. Despite these advancements, all the above methods essentially perform 2D segmentation when conducting open-vocabulary segmentation, as they compare rendered 2D language features with the input text query embedding.

OpenGaussian [32] leverages contrastive learning to assign a feature embedding to each Gaussian, then applies K -means clustering to group Gaussians into multiple object clusters, thereby realizing 3D segmentation. Similarly, GaussianCut [6] utilizes graphcut [1, 4, 5] to segment Gaussians into foreground and background based on user input.

However, all of the above-mentioned methods adhere to a “splat then segment” (*i.e.* reconstruction then segmentation) pipeline, which inherently results in imprecise object boundaries, since each Gaussian may contain geometry and semantic information from different objects. Furthermore, these methods struggle with dynamic scenes due to Gaussian-object misalignment, preventing their direct application to non-static environments. Dynamic 3D Gaussian Distillation (DGD) [11] distills the feature from LSeg [12] into a feature field to achieve open-vocabulary segmentation, however it still suffers from object-Gaussian misalignment issue as it does not explicitly handle it.

In contrast, we introduce *Segment then Splat*, which overturns the long-established “splat then segment” paradigm. Instead, our approach first initializes object-specific Gaussians for each object before performing the reconstruction process. By enforcing object-Gaussian correspondence, our method achieves more accurate object geometries and compatibility with dynamic scenes.

3. Method

We introduce *Segment then Splat*, a unified approach for 3D open-vocabulary segmentation based on Gaussian Splatting, as illustrated in Fig. 2. The process begins by extracting multi-view masks for each object through a *robust object tracking* module (Sec. 3.2), ensuring reliable detection and mask generation. Next, each Gaussian initialized by COLMAP [25, 26] is assigned an object ID according to these masks, partitioning the entire scene into multiple *object-specific Gaussian sets* (Sec. 3.3). During *optimization & reconstruction* (Sec. 3.4), each Gaussian contributes exclusively to its assigned object, preserving Gaussian-object correspondence and resulting in more accurate object geometries. After reconstruction, *CLIP*

embeddings are associated with each group of Gaussians (Sec. 3.5), enabling open-vocabulary queries. Besides, three levels of granularity (large, middle, and small) are introduced to facilitate object retrieval at different scales.

3.1. Preliminary: 3D and 4D Gaussian Splatting

3DGS. 3D Gaussian Splatting represents a scene using a collection of 3D ellipsoids, each modeled as an anisotropic 3D Gaussian. Each Gaussian is parameterized by a mean x , which defines the center of the ellipsoid, a covariance matrix Σ , which determines its shape, as shown in Eq. (1). The color of the Gaussian is defined using spherical harmonics.

$$G(x) = e^{-\frac{1}{2}(x)^T \Sigma^{-1}(x)} \quad (1)$$

During rendering, the 3D Gaussians are first transformed into camera coordinates and projected onto the image plane as 2D Gaussians. The final pixel color is then computed through alpha blending, which integrates the weighted Gaussian colors from front to back:

$$\hat{C} = \sum_{i \in \mathcal{N}} c_i \alpha_i \prod_{j=1}^{i-1} (1 - \alpha_j), \quad (2)$$

where c_i is the color of each Gaussian, and α_i is the alpha value of the i^{th} Gaussian.

4DGS. 4D Gaussian Splatting is an extension of 3D Gaussian Splatting, capable of modeling dynamic scenes. Following Deformable 3D Gaussian Splatting [33], we incorporate a deformation field to capture scene dynamics:

$$(\delta x, \delta r, \delta s) = \mathcal{F}_\theta(\gamma(x), \gamma(t)), \quad (3)$$

where \mathcal{F}_θ represents deformation field, which takes Gaussian mean x and time t as input and outputs the deformation $(\delta x, \delta r, \delta s)$ at time t . $\gamma(\cdot)$ denotes positional encoding.

3.2. Robust Object Tracking

Given a set of input images $\{I_i\}_{i=0}^n$, our goal is to extract multi-view masks for all objects at different granularity levels (*i.e.* large, middle and small) in the scene. We begin by leveraging Segment Anything (SAM) [10] with grid-based point prompting to obtain initial static object masks of different granularities in the first input frame I_0 . Subsequently, SAM2 [24] is employed to track objects throughout the sequence based on the extracted mask from I_0 . However, this process presents several challenges: 1) Some objects may not appear in the first frame, leading to their exclusion from tracking. 2) Due to grid-based prompting, one pixel may be tracked multiple times into different masks, either belonging to a single object or a part of an object. 3) If an object temporarily disappears and reappears later in the scene, tracking may be lost. To address these issues, we propose several post-processing strategies.

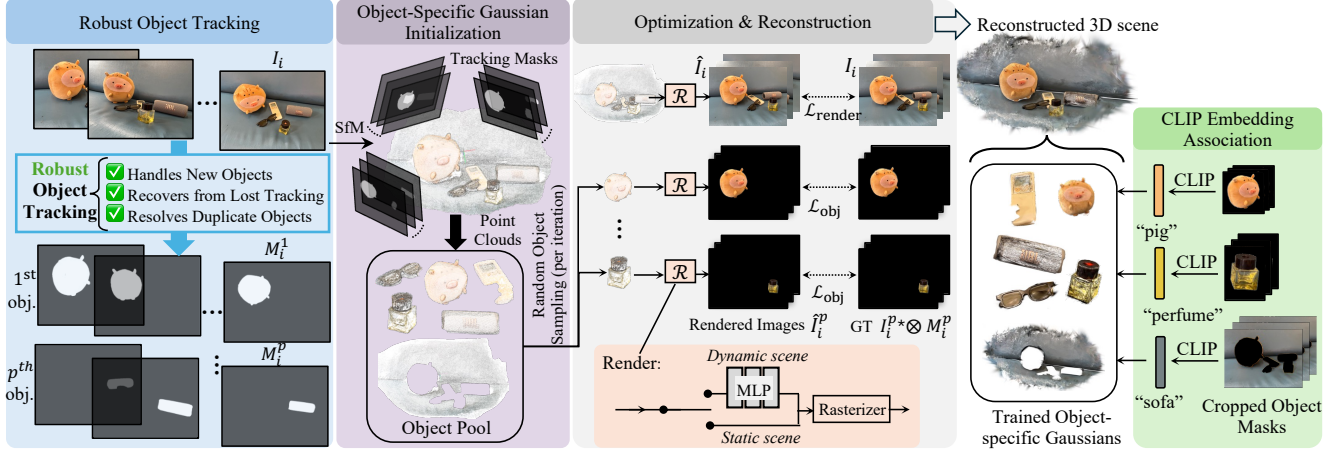


Figure 2. **A detailed demonstration of our proposed Segment then Splat pipeline.** Our approach first extracts multi-view masks for each object through a robust tracking module, then object IDs are assigned to each initial Gaussian based on these masks, forming distinct object-specific sets. During optimization, object specific loss \mathcal{L}_{obj} is used to enforce Gaussian-object correspondence and thus resulting in more accurate object geometries. Finally, we associate each Gaussian group with CLIP embeddings, enabling open-vocabulary queries.

Detect Any New Objects. To ensure newly appearing objects are captured, we introduce a detection mechanism at fixed intervals of Δt . Specifically, we compare the ratio of the segmented region in frame $I_{t+\Delta t}$ to that in frame I_t . A significant decline in this ratio indicates the potential presence of new objects. At this point, we re-segment the scene and analyze the intersection between the new and previous segmentation results. Objects with minimal overlap with prior masks are identified as new objects and added to the static segmentation results. SAM2 then continues tracking based on this updated segmentation.

Resolving Multiple Trackings of a Pixel. To ensure that each pixel is assigned to only one object within a given granularity level, we employ an Intersection over Union (IoU)-based filtering approach. For each pair of masks in I_i , if their IoU exceeds a predefined threshold, the smaller object is discarded in favor of the larger one, as it can be segmented separately at a finer granularity level.

Handling Lost Tracking. When an object’s tracking is lost, it may be incorrectly treated as a new object upon its reappearance in subsequent frames, leading to multiple instances representing the same object. In these scenarios, we resolve this issue using the approach described in Sec. 3.3.

3.3. Object-Specific Gaussian Initialization

As our method follows a “segmentation then reconstruction” strategy, we first segment the Gaussians initialized by COLMAP into distinct sets, each representing a different object. Each Gaussian is assigned three object IDs, corresponding to three granularity levels. To determine these IDs, we analyze the visibility of each Gaussian center across all views and identify the corresponding object mask region

in which it resides. After object IDs are determined, we handle the lost tracking issue stated in Sec. 3.2. When an object is tracked multiple times as different instances, the corresponding Gaussians should share a similar geometric center and appearance (e.g. color). Therefore, we refine the segmentation by merging Gaussians and its corresponding object mask, if they exhibit a closely aligned “geometric-appearances distance”, defined as follows:

$$d(\mathbf{G}_i, \mathbf{G}_j) = \lambda_d |\overline{\mathbf{M}}_i - \overline{\mathbf{M}}_j|_2 + (1 - \lambda_d) |\overline{\mathbf{C}}_i - \overline{\mathbf{C}}_j|_2, \quad (4)$$

where \mathbf{G}_i and \mathbf{G}_j are two sets of Gaussians representing different objects, $\overline{\mathbf{M}}_i$ and $\overline{\mathbf{M}}_j$ denote the mean Gaussian centers, representing object geometric centers, and $\overline{\mathbf{C}}_i$ and $\overline{\mathbf{C}}_j$ are the average colors of the respective Gaussian sets. λ_d is the weight to balance geometric distance and appearance distance. Additionally, since COLMAP provides only a sparse reconstruction of the scene, some objects may not be covered and thus lack corresponding Gaussians. We compensate these missing objects by randomly initializing Gaussians. Furthermore, we generate a set of background Gaussians to fill small unsegmented regions.

3.4. Optimization & Reconstruction

Optimization Goal. After initializing Gaussians as distinct object sets, they are used to reconstruct the scene. During this process, we enforce constraints to ensure that each set of Gaussians contributes only to its corresponding object. Specifically, we introduce an additional object-level loss term, denoted as \mathcal{L}_{obj} , alongside the standard rendering loss \mathcal{L}_{render} :

$$\mathcal{L}_{render} = (1 - \lambda_r) \mathcal{L}_1(\hat{I}_i, I_i) + \lambda_r \mathcal{L}_{DSSIM}(\hat{I}_i, I_i), \quad (5)$$

$$\mathcal{L}_{\text{obj}} = \mathcal{L}_1(M_i^p \otimes I_i, \hat{I}_i^p), \quad (6)$$

where \hat{I}_i is the rendered i^{th} image, and \hat{I}_i^p and M_i^p represent the rendered p^{th} object in the i^{th} image and its corresponding mask, respectively, as extracted in Sec. 3.2. The overall loss function is as follows:

$$\mathcal{L} = \mathcal{L}_{\text{render}} + \mathcal{L}_{\text{obj}}. \quad (7)$$

Throughout the entire reconstruction process, all densification and cloning operations are performed strictly within each object-specific Gaussian set, preserving the Gaussian-object correspondence. Additionally, we implement a Gaussian persistence mechanism to ensure that each set of object-specific Gaussians is not completely pruned, thereby preventing scenarios where an object could lose all its associated Gaussians.

Optimization Efficiency. Since the number of objects in a scene can range from a few to over a hundred, computing \mathcal{L}_{obj} for every object becomes computationally infeasible, as it would require K times more rendering operations per iteration. To address this, we randomly sample m objects per iteration to apply \mathcal{L}_{obj} , balancing efficiency and optimization effectiveness.

Optimization on Multiple Granularities. Noticed that we have three level granularities: large, middle and small. To ensure effective optimization, we must account for these varying scales when determining the optimization order. Since smaller objects are always part of larger ones, they should be optimized first. If the order is reversed, *i.e.* optimizing smaller objects after larger ones, the internal structure of the larger objects may become disorganized again, as shown in Fig. 3. Thus the \mathcal{L}_{obj} will finally be formulated as:

$$\mathcal{L}_{\text{obj}} = \begin{cases} \mathcal{L}_{\text{obj},S}, & \text{stage1} \\ \mathcal{L}_{\text{obj},S} + \mathcal{L}_{\text{obj},M}, & \text{stage2} \\ \mathcal{L}_{\text{obj},S} + \mathcal{L}_{\text{obj},M} + \mathcal{L}_{\text{obj},L}, & \text{stage3} \end{cases}, \quad (8)$$

where $\mathcal{L}_{\text{obj},S}$, $\mathcal{L}_{\text{obj},M}$, $\mathcal{L}_{\text{obj},L}$ represent per-object loss for small, middle, large level respectively.

Partial Mask Filtering. In 3D-aware segmentation, objects can be reconstructed even from views where they would typically appear occluded. Consequently, multi-view 2D masks provided as supervision can introduce discrepancies, as they do not account for occluded regions revealed during rendering, as shown in Fig. 5. This discrepancy can lead to incorrect constraints, ultimately distorting the geometric structure of the 3D objects. The original Gaussian Splatting (3DGS) framework can partially resolve this issue by leveraging multi-view consistency, but errors from unreliable masks persists. To robustly address this, we propose a partial mask filtering strategy applied at the end of training. Specifically, we render each reconstructed object into

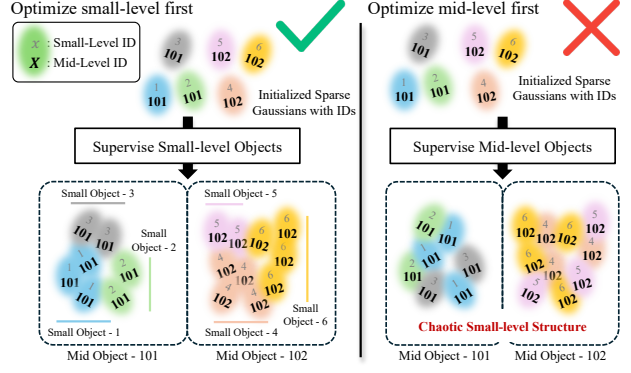


Figure 3. A demonstration of how the optimization order of different granularity will affect the reconstruction result. When small-level objects are optimized first, the structures of both small-level and middle-level objects are well-preserved. In contrast, optimizing middle-level objects first results in well-maintained middle-level structures but chaotic internal structures at the small level due to the absence of supervision.

2D images, compute their Intersection-over-Union (IoU) against the provided masks, and discard masks exhibiting low IoU scores. This ensures that only consistent, accurate masks inform the final optimization, significantly enhancing the geometric fidelity of the reconstructed 3D objects.

3.5. CLIP Embedding Association

Unlike previous methods [9, 21, 28, 36] that supervise Gaussian language embeddings indirectly via 2D feature maps, leading to inconsistent embeddings for Gaussians belonging to the same object, our approach directly assigns a unified language embedding to each object-specific Gaussian set. This ensures consistent semantic embeddings within each object, significantly improving segmentation accuracy and boundary precision. The CLIP embedding of each object is calculated as follows:

$$f_p = \frac{1}{n} \sum_{M_i^p \notin M_{\text{part}}^p} \text{CLIP}_i(\text{crop}(M_i^p \otimes I_i)), \quad (9)$$

where f_p is the language embedding of the p^{th} object, M_{part}^p is the partial masks that excluded in the previous section. $\text{CLIP}_i(\cdot)$ represents the CLIP image encoder and $\text{crop}(\cdot)$ denotes the cropping function to extract the mask region.

3.6. Open-Vocabulary Query

Given an input text prompt, we perform open vocabulary query following the below strategy:

$$f_q = \text{CLIP}_t(q), \quad (10)$$

$$q_{\text{return}} = \arg \max_p \cos(f_q, f_p), \quad (11)$$

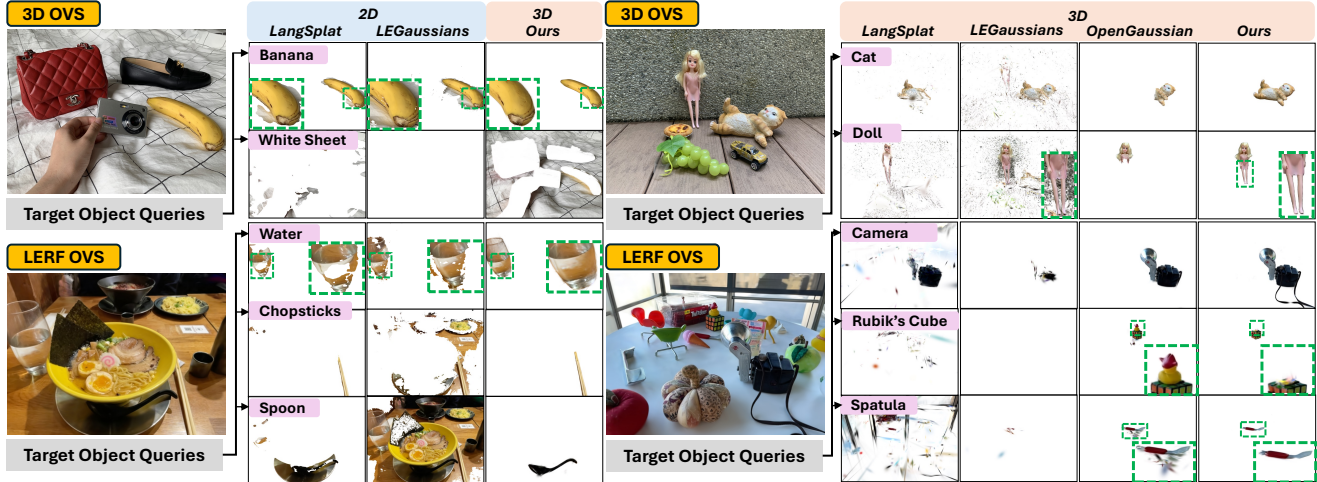


Figure 4. **Qualitative comparison on static scenes.** Compared to baseline methods, our approach accurately retrieves the correct object and produces sharper segmentation boundaries. In contrast, 2D pixel-based methods exhibit ambiguous boundaries, while OpenGaussian either misses parts of the object or incorrectly groups irrelevant objects together.

where f_q is the CLIP embedding of the input text prompt q , given by CLIP text encoder $\text{CLIP}_t(\cdot)$, and q_{return} is the object that best matches the query, determined by maximizing the cosine similarity $\cos(\cdot)$ between the query embedding and the object embeddings.

4. Experiments

4.1. Dataset

To assess the segmentation performance of our proposed method, we conduct experiments on two static scene datasets (i.e., 3DOVS dataset [15] and LERF_OVS dataset [9]) and two dynamic scene datasets (i.e., HyperNeRF dataset [20] and Plenoptic Video dataset [13]).

4.2. Implementation Details

The new object detection stride Δt in the robust object tracking module is set to 10. Following the original 3DGS implementation, we set λ_r in $\mathcal{L}_{\text{render}}$ to 0.2. For λ_d , which balances geometric distance and appearance distance in Eq. (4), we use a value of 0.5. During each iteration, we sample one object per granularity for 3DOVS to compute \mathcal{L}_{obj} and three objects per granularity for all the remaining datasets. The mIoU threshold for partial mask filtering is set to 70%. For the 3DOVS dataset, given its smaller scale, we train for 20,000 iterations (5,000 for stage1, 5,000 for stage2, and the remaining for stage3), and introducing partial mask filtering in the last 5,000 iterations. For larger-scale datasets (i.e. LERF_OVS, HyperNeRF, and Plenoptic), training extends to 40,000 iterations (5,000 for stage1, 5,000 for stage2, and the remaining for stage3), with partial mask filtering applied during the last 10,000 iterations.

4.3. Baselines and Evaluation Metrics

Baselines. We categorize the baselines into two groups based on their querying strategies: 2D pixel-based segmentation and 3D-based segmentation. For static scenes, we use LangSplat [21] and LEGaussians [21] as the 2D pixel-based baselines. For the 3D baselines, we choose OpenGaussian[32], and we also adapt LangSplat and LEGaussians for 3D segmentation to evaluate their performance. In dynamic scenes, we adopt a zero-shot image segmentation model CLIP-LSeg [12] as the 2D pixel-based baseline and DGD [11] as the 3D-based approach.

Evaluation Metrics. We adopt mean intersection over union (mIoU) as evaluation metric for open-vocabulary segmentation task. For training efficiency, since all baselines and our proposed method share a similar preprocessing pipeline, we only focus on comparing the optimization time. All the time in the tables are measured in minutes. One thing to be mentioned is that, due to the nature of 3D segmentation and the evaluation used for open-vocabulary segmentation, there is a slight reduction in our mIoU score. This is because 3D segmentation directly retrieves the Gaussians associated with an object, revealing occluded parts that are not visible in some ground truth masks, as shown in Fig. 5.

4.4. Open-Vocabulary Query

Results on 3DOVS dataset. The quantitative results on the 3DOVS dataset are presented in Tab. 1. Our method outperforms all baseline approaches. The qualitative comparison is shown in Fig. 4. Notably, 2D pixel-based methods tend to produce relatively ambiguous boundaries, whereas our approach, leveraging the “segment then splat” strat-

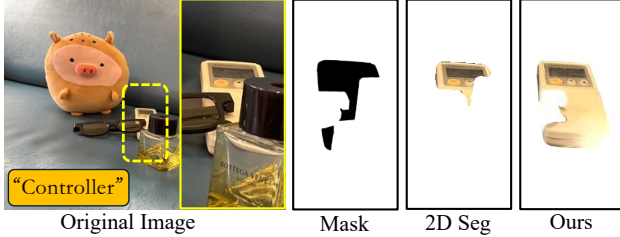


Figure 5. Comparison between 2D pixel-based segmentation and our 3D segmentation. Unlike 2D pixel-based methods, which are limited by occlusions, our approach can retrieve the complete object even from an occluded view.

Table 1. Quantitative segmentation results on **static scenes**.

		LERF_OVS		3DOVS	
Method		mIoU \uparrow	Time \downarrow	mIoU \uparrow	Time \downarrow
2D	LangSplat [21]	46.37	62.00	82.49	68.90
	LEGaussians [28]	18.79	72.00	52.12	55.90
3D	LangSplat [21]	16.76	62.00	47.31	68.90
	LEGaussian [28]	12.08	72.00	33.44	55.90
	OpenGaussian [32]	42.43	69.75	31.00	59.40
	Ours	52.10	50.75	88.53	9.40

egy, achieves significantly clearer object boundaries. For 3D segmentation methods, OpenGaussian requires a predefined number of objects K for clustering. Since 3DOVS contains fewer objects compared to LERF_OVS, we manually reduced its preset K . However, even after this adjustment, OpenGaussian still only retrieves parts of certain objects. Although LangSplat and LEGaussians are modified to segment Gaussians instead of pixels, their performance remains suboptimal. This is because the language embedding of each Gaussian is not directly supervised and may encode multiple semantics from different objects, leading to inaccurate segmentation results. Additionally, since our method follows a single-pass reconstruction process and the scene scale is relatively small, our training time is significantly shorter compared to the baseline methods.

Results on LERF_OVS dataset. The quantitative results on the LERF_OVS dataset are also presented in Tab. 1 and the qualitative results are shown in Fig. 4. Similar to the 3DOVS dataset, 2D pixel-based methods produce less precise object boundaries, while our method demonstrates significantly improved results. For 3D-based methods, OpenGaussian performs much better on LERF_OVS compared to 3DOVS. However, since OpenGaussian requires a predefined number of clusters, some objects may be incorrectly grouped together (e.g., the rubber duck and the Rubik’s cube). Moreover, due to its “splat then segmentation” strategy, its object boundaries remain less accurate than those

Table 2. Quantitative segmentation results on **dynamic scenes**.

		HyperNeRF		Planoptic	
Method		mIoU \uparrow	Time \downarrow	mIoU \uparrow	Time \downarrow
2D	LSeg [12]	15.71	-	1.49	-
3D	DGD [11]	7.83	1564.5	1.65	1733
	Ours	69.48	218	44.00	161.3

produced by our *Segment then Splat* method.

Results on HyperNeRF dataset. The quantitative results and qualitative results on HyperNeRF dataset are presented in Tab. 2 and Sec. 4.4 respectively. Since our method explicitly enforces Gaussian-object correspondence, it can be directly applied to dynamic scenes, achieving good segmentation performance without the Gaussian-object misalignment issue encountered by previous approaches. In contrast, methods such as DGD, which relies on learning a language field supervised via 2D feature maps, suffer from misalignment, as a single Gaussian might represent multiple distinct objects across different time steps. As illustrated in Fig. 6, this misalignment results in retrieving irrelevant Gaussians. Moreover, because DGD does not directly supervise the language embeddings of each Gaussian, Gaussians located far apart may share similar embeddings, further deteriorating segmentation quality. In addition, our method achieves nearly a ten-fold improvement in optimization speed compared to DGD, as learning a dynamic language field is computationally intensive. We omit training time results for LSeg, as it is a zero-shot segmentation method requiring no additional optimization.

Results on Plenoptic Video dataset. Quantitative results and qualitative results are shown in Tab. 2 and Fig. 6. Similar to the observations on the HyperNeRF dataset, many irrelevant Gaussians are retrieved due to object-Gaussian misalignment issue and the “splat then segment” strategy. Besides, both LSeg and DGD fail when retrieving small objects (e.g. bunny painting).

4.5. Ablation Study

Number of Objects to Supervise. In this ablation study, we examine the relationship between the number of supervised objects in each granularity per iteration and the segmentation performance. We pick two static scenes from LERF_OVS dataset and two dynamic scenes from HyperNeRF dataset. The results are presented in Tab. 3. As expected, increasing the number of supervised objects per iteration generally enhances segmentation performance. However, beyond a certain threshold, the performance gain becomes marginal. For scenes with fewer objects (e.g. chickchicken and split-cookie), performance quickly converges after a certain number of supervised objects. In contrast, more complex scenes containing many objects (e.g.

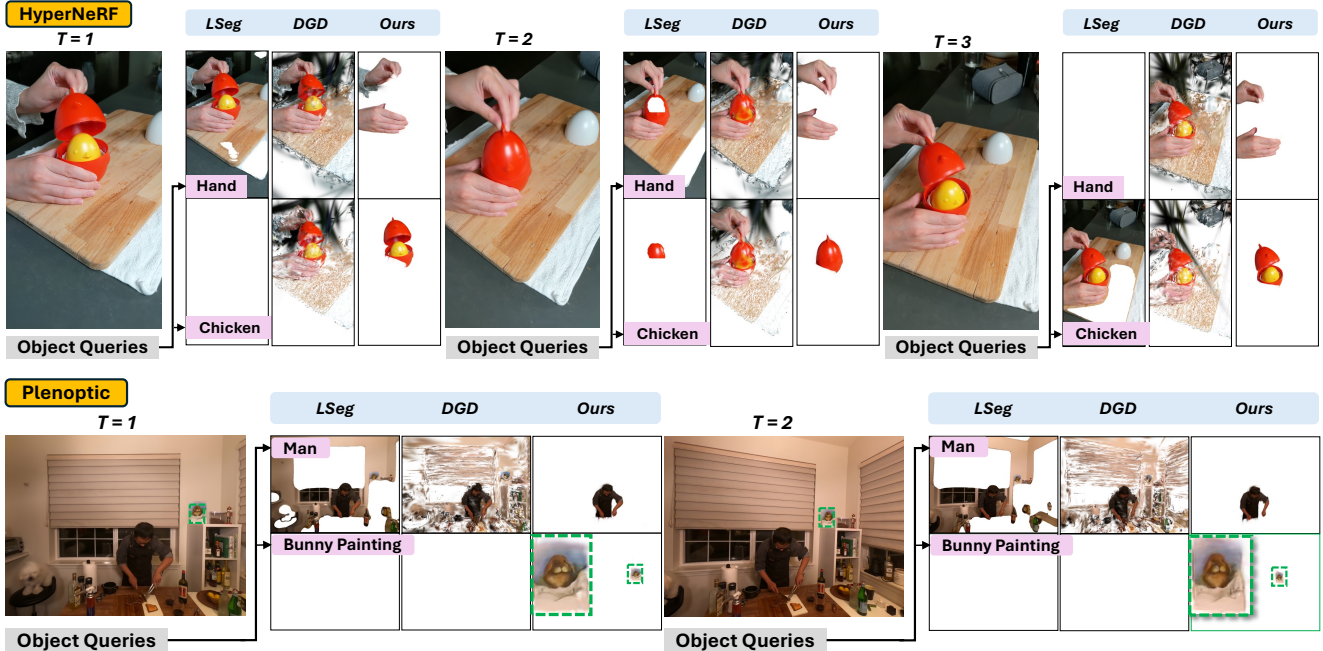


Figure 6. **Qualitative comparison on dynamic scenes.** As our method enforce object-Gaussian correspondence, it can be directly applied to dynamic scenes and achieve good performance, whereas DGD and LSeg tend to include irrelevant content and are not able to retrieve small objects (e.g. bunny painting).

Table 3. Ablation study on the number of supervised objects per iteration at each granularity level. As the number of supervised objects increases, we observe an improvement in segmentation performance, but also an increase in training time.

	Static Scene				Dynamic Scene			
	ramen		waldo_kitchen		chickchicken		split-cookie	
# obj	Time↓	mIoU↑	Time↓	mIoU↑	Time↓	mIoU↑	Time↓	mIoU↑
1	26	51.09	44	33.97	146	73.11	180	77.76
3	34	54.38	48	40.71	157	74.89	202	80.30
5	42	55.61	54	40.83	172	75.29	253	80.47
7	53	56.03	63	40.77	185	75.21	258	81.52
9	62	56.48	68	41.59	201	75.23	309	81.74

ramen and waldo_kitchen) continue to show performance improvements, though at a diminished rate. Additionally, training time increases proportionally with the number of supervised objects. To balance training time and segmentation performance, we choose three objects for LERF_OVS, Plenoptic and HyperNeRF in our experiments.

Partial Mask Filtering. In this ablation study, we investigate the impact of the partial mask filtering strategy on both segmentation performance and reconstruction quality. As shown in Tab. 4, scenes with a larger number of objects (e.g., ramen and waldo_kitchen) tend to have more occluded views, leading to a more significant performance improvement when applying partial mask filtering. In contrast, scenes with fewer objects (e.g., chickchicken and

Table 4. Ablation study on the partial mask filtering strategy, w/o MF stands for without partial mask filtering.

Method	Static Scene				Dynamic Scene			
	ramen		waldo_kitchen		chickchicken		split-cookie	
	mIoU↑	PSNR↑	mIoU↑	PSNR↑	mIoU↑	PSNR↑	mIoU↑	PSNR↑
w/o MF	42.19	23.11	31.94	30.43	72.65	29.32	80.23	32.76
ours	54.38	24.54	40.71	31.33	74.89	29.62	80.30	33.04

split-cookie) exhibit a smaller performance gain. Overall, the results validate the effectiveness of our proposed partial mask filtering strategy in improving segmentation accuracy, particularly in complex scenes with high object density.

5. Conclusion

We propose **Segment then Splat**, a unified framework for 3D open-vocabulary segmentation based on Gaussian Splatting. We reverse the long-established “segmentation after reconstruction” approach to form a “segmentation then reconstruction” pipeline. By enforcing object-Gaussian correspondence through the entire process, **Segment then Splat** yields a better object boundary and can be directly applied to dynamic scenes. Finally, open-vocabulary querying is enabled by assigning each object-specific Gaussian group with a unified CLIP embedding. Extensive experiments on various static and dynamic scene datasets demonstrate the superior performance of our method.

References

- [1] Yuri Y Boykov and M-P Jolly. Interactive graph cuts for optimal boundary & region segmentation of objects in nd images. In *Proceedings eighth IEEE international conference on computer vision. ICCV 2001*, pages 105–112. IEEE, 2001. 3
- [2] Ang Cao and Justin Johnson. Hexplane: A fast representation for dynamic scenes. In *Proceedings of the IEEE/CVF Conference on Computer Vision and Pattern Recognition*, pages 130–141, 2023. 2
- [3] Yiwen Chen, Zilong Chen, Chi Zhang, Feng Wang, Xiaofeng Yang, Yikai Wang, Zhongang Cai, Lei Yang, Huaping Liu, and Guosheng Lin. Gaussianeditor: Swift and controllable 3d editing with gaussian splatting. In *Proceedings of the IEEE/CVF conference on computer vision and pattern recognition*, pages 21476–21485, 2024. 1
- [4] Lester Randolph Ford and Delbert Ray Fulkerson. Flows in networks. 2015. 3
- [5] Andrew V Goldberg and Robert E Tarjan. A new approach to the maximum-flow problem. *Journal of the ACM (JACM)*, 35(4):921–940, 1988. 3
- [6] Umangi Jain, Ashkan Mirzaei, and Igor Gilitschenski. Gaussiancut: Interactive segmentation via graph cut for 3d gaussian splatting. *Advances in Neural Information Processing Systems*, 37:89184–89212, 2025. 2, 3
- [7] Nikhil Keetha, Jay Karhade, Krishna Murthy Jatavallabhula, Gengshan Yang, Sebastian Scherer, Deva Ramanan, and Jonathon Luiten. Splatam: Splat track & map 3d gaussians for dense rgb-d slam. In *Proceedings of the IEEE/CVF Conference on Computer Vision and Pattern Recognition*, pages 21357–21366, 2024. 1
- [8] Bernhard Kerbl, Georgios Kopanas, Thomas Leimkühler, and George Drettakis. 3d gaussian splatting for real-time radiance field rendering. *ACM Transactions on Graphics*, 42(4), 2023. 2
- [9] Justin* Kerr, Chung Min* Kim, Ken Goldberg, Angjoo Kanazawa, and Matthew Tancik. Lrf: Language embedded radiance fields. In *International Conference on Computer Vision (ICCV)*, 2023. 2, 5, 6
- [10] Alexander Kirillov, Eric Mintun, Nikhila Ravi, Hanzi Mao, Chloe Rolland, Laura Gustafson, Tete Xiao, Spencer Whitehead, Alexander C Berg, Wan-Yen Lo, et al. Segment anything. In *Proceedings of the IEEE/CVF international conference on computer vision*, pages 4015–4026, 2023. 3
- [11] Isaac Labe, Noam Issachar, Itai Lang, and Sagie Benaim. Dgd: Dynamic 3d gaussians distillation. In *European Conference on Computer Vision*, pages 361–378. Springer, 2024. 3, 6, 7
- [12] Boyi Li, Kilian Q Weinberger, Serge Belongie, Vladlen Koltun, and René Ranftl. Language-driven semantic segmentation. *arXiv preprint arXiv:2201.03546*, 2022. 3, 6, 7
- [13] Tianye Li, Mira Slavcheva, Michael Zollhoefer, Simon Green, Christoph Lassner, Changil Kim, Tanner Schmidt, Steven Lovegrove, Michael Goesele, Richard Newcombe, et al. Neural 3d video synthesis from multi-view video. *Proceedings of the IEEE/CVF conference on computer vision and pattern recognition*, pages 5521–5531, 2022. 6
- [14] Zhan Li, Zhang Chen, Zhong Li, and Yi Xu. Spacetime gaussian feature splatting for real-time dynamic view synthesis. In *Proceedings of the IEEE/CVF Conference on Computer Vision and Pattern Recognition*, pages 8508–8520, 2024. 2
- [15] Kunhao Liu, Fangneng Zhan, Jiahui Zhang, Muyu Xu, Yingchen Yu, Abdulmoteleb El Saddik, Christian Theobalt, Eric Xing, and Shijian Lu. Weakly supervised 3d open-vocabulary segmentation. *Advances in Neural Information Processing Systems*, 36:53433–53456, 2023. 6
- [16] Yiren Lu, Jing Ma, and Yu Yin. View-consistent object removal in radiance fields. In *Proceedings of the 32nd ACM International Conference on Multimedia*, pages 3597–3606, 2024. 1
- [17] Yiren Lu, Yunlai Zhou, Disheng Liu, Tuo Liang, and Yu Yin. Bard-gs: Blur-aware reconstruction of dynamic scenes via gaussian splatting. *arXiv preprint arXiv:2503.15835*, 2025. 2
- [18] Jonathon Luiten, Georgios Kopanas, Bastian Leibe, and Deva Ramanan. Dynamic 3d gaussians: Tracking by persistent dynamic view synthesis. In *2024 International Conference on 3D Vision (3DV)*, pages 800–809. IEEE, 2024. 2
- [19] Hidenobu Matsuki, Riku Murai, Paul HJ Kelly, and Andrew J Davison. Gaussian splatting slam. In *Proceedings of the IEEE/CVF Conference on Computer Vision and Pattern Recognition*, pages 18039–18048, 2024. 1
- [20] Keunhong Park, Utkarsh Sinha, Peter Hedman, Jonathan T. Barron, Sofien Bouaziz, Dan B Goldman, Ricardo Martin-Brualla, and Steven M. Seitz. Hypernerf: A higher-dimensional representation for topologically varying neural radiance fields. *ACM Trans. Graph.*, 40(6), 2021. 6
- [21] Minghan Qin, Wanhua Li, Jiawei Zhou, Haoqian Wang, and Hanspeter Pfister. Langsplat: 3d language gaussian splatting. In *Proceedings of the IEEE/CVF Conference on Computer Vision and Pattern Recognition*, pages 20051–20060, 2024. 2, 3, 5, 6, 7
- [22] Alec Radford, Jong Wook Kim, Chris Hallacy, Aditya Ramesh, Gabriel Goh, Sandhini Agarwal, Girish Sastry, Amanda Askell, Pamela Mishkin, Jack Clark, et al. Learning transferable visual models from natural language supervision. In *International conference on machine learning*, pages 8748–8763. PmlR, 2021. 2
- [23] Adam Rashid, Satvik Sharma, Chung Min Kim, Justin Kerr, Lawrence Yunliang Chen, Angjoo Kanazawa, and Ken Goldberg. Language embedded radiance fields for zero-shot task-oriented grasping. In *7th Annual Conference on Robot Learning*, 2023. 1
- [24] Nikhila Ravi, Valentin Gabeur, Yuan-Ting Hu, Ronghang Hu, Chaitanya Ryali, Tengyu Ma, Haitham Khedr, Roman Rädle, Chloe Rolland, Laura Gustafson, Eric Mintun, Junting Pan, Kalyan Vasudev Alwala, Nicolas Carion, Chao-Yuan Wu, Ross Girshick, Piotr Dollár, and Christoph Feichtenhofer. Sam 2: Segment anything in images and videos. *arXiv preprint arXiv:2408.00714*, 2024. 3
- [25] Johannes Lutz Schönberger and Jan-Michael Frahm. Structure-from-motion revisited. In *Conference on Computer Vision and Pattern Recognition (CVPR)*, 2016. 3

- [26] Johannes Lutz Schönberger, Enliang Zheng, Marc Pollefeys, and Jan-Michael Frahm. Pixelwise view selection for unstructured multi-view stereo. In *European Conference on Computer Vision (ECCV)*, 2016. 3
- [27] William Shen, Ge Yang, Alan Yu, Jansen Wong, Leslie Pack Kaelbling, and Phillip Isola. Distilled feature fields enable few-shot language-guided manipulation. In *7th Annual Conference on Robot Learning*, 2023. 1
- [28] Jin-Chuan Shi, Miao Wang, Hao-Bin Duan, and Shao-Hua Guan. Language embedded 3d gaussians for open-vocabulary scene understanding. In *Proceedings of the IEEE/CVF Conference on Computer Vision and Pattern Recognition*, pages 5333–5343, 2024. 2, 3, 5, 7
- [29] Can Wang, Menglei Chai, Mingming He, Dongdong Chen, and Jing Liao. Clip-nerf: Text-and-image driven manipulation of neural radiance fields. In *Proceedings of the IEEE/CVF conference on computer vision and pattern recognition*, pages 3835–3844, 2022. 1
- [30] Junjie Wang, Jiemin Fang, Xiaopeng Zhang, Lingxi Xie, and Qi Tian. Gaussianeditor: Editing 3d gaussians delicately with text instructions. In *Proceedings of the IEEE/CVF conference on computer vision and pattern recognition*, pages 20902–20911, 2024. 1
- [31] Guanjun Wu, Taoran Yi, Jiemin Fang, Lingxi Xie, Xiaopeng Zhang, Wei Wei, Wenyu Liu, Qi Tian, and Xinggang Wang. 4d gaussian splatting for real-time dynamic scene rendering. In *Proceedings of the IEEE/CVF conference on computer vision and pattern recognition*, pages 20310–20320, 2024. 2
- [32] Yanmin Wu, Jiarui Meng, Haijie Li, Chenming Wu, Yahao Shi, Xinhua Cheng, Chen Zhao, Haocheng Feng, Errui Ding, Jingdong Wang, et al. Opengaussian: Towards point-level 3d gaussian-based open vocabulary understanding. *arXiv preprint arXiv:2406.02058*, 2024. 2, 3, 6, 7
- [33] Ziyi Yang, Xinyu Gao, Wen Zhou, Shaohui Jiao, Yuqing Zhang, and Xiaogang Jin. Deformable 3d gaussians for high-fidelity monocular dynamic scene reconstruction. In *Proceedings of the IEEE/CVF conference on computer vision and pattern recognition*, pages 20331–20341, 2024. 2, 3
- [34] Zeyu Yang, Hongye Yang, Zijie Pan, and Li Zhang. Real-time photorealistic dynamic scene representation and rendering with 4d gaussian splatting. In *International Conference on Learning Representations (ICLR)*, 2024. 2
- [35] Wenbo Zhang, Lu Zhang, Ping Hu, Liqian Ma, Yunzhi Zhuge, and Huchuan Lu. Bootstrapping clustering of gaussians for view-consistent 3d scene understanding. *arXiv preprint arXiv:2411.19551*, 2024. 2
- [36] Shijie Zhou, Haoran Chang, Sicheng Jiang, Zhiwen Fan, Zehao Zhu, Dejie Xu, Pradyumna Chari, Suyu You, Zhangyang Wang, and Achuta Kadambi. Feature 3dgs: Supercharging 3d gaussian splatting to enable distilled feature fields. In *Proceedings of the IEEE/CVF Conference on Computer Vision and Pattern Recognition*, pages 21676–21685, 2024. 2, 5
- [37] Xingxing Zuo, Pouya Samangouei, Yunwen Zhou, Yan Di, and Mingyang Li. Fmgs: Foundation model embedded 3d gaussian splatting for holistic 3d scene understanding. *International Journal of Computer Vision*, pages 1–17, 2024. 2